Scientific Research Publishing

Open Journal of Fluid Dynamics, 2023, 13, 191-205
https://www.scirp.org/journal/ojfd
ISSN Online: 2165-3860
ISSN Print: 2165-3852

Numerical Simulation of Saint-Venant Equations with Thermal Energy Dependency: Applications on Global Warming

Raphael de O. Garcia[1], Graciele P. Silveira[2]

[1]Department of Actuarial Science, Federal University of São Paulo, Osasco, Brazil
[2]Department of Physics, Chemistry and Mathematics, Federal University of São Carlos, Sorocaba, Brazil
Email: rogarcia@unifesp.br, graciele@ufscar.br

How to cite this paper: de O. Garcia, R. and Silveira, G.P. (2023) Numerical Simulation of Saint-Venant Equations with Thermal Energy Dependency: Applications on Global Warming. *Open Journal of Fluid Dynamics*, **13**, 191-205.
https://doi.org/10.4236/ojfd.2023.134014

Received: August 16, 2023
Accepted: September 22, 2023
Published: September 25, 2023

Abstract

Since the Industrial Revolution, humanity has been intensifying the burning of fossil fuels and as a consequence, the average temperature on Earth has been increasing. The 20th century was the warmest and future prospects are not favorable, that is, even higher temperatures are expected. This demonstrates the importance of studies on the subject, mainly to predict possible environmental, social and economic consequences. The objective of this work was to identify the interference of the increase in ambient temperature in the dynamics of fluids, such as ocean waves advancing over the continent. For this, thermal energy was considered in the Saint-Venant equations and computational implementations were performed via Lax-Friedrichs and Adams-Moulton methods. The results indicated that, in fact, depending on the amount of thermal energy transferred to the fluid, the advance of water towards the continent can occur, even in places where such a phenomenon has never been observed.

Keywords

Computational Fluid Dynamics, Saint-Venant Equations, Numerical Methods, Global Warming

1. Introduction

In recent decades, discussions about climate change have been in evidence, mainly because its consequences are causing urgent environmental, social and economic problems.

The Intergovernmental Panel on Climate Change (IPCC) was created in 1988, within the framework of the United Nations, to synthesize and disseminate the

most advanced knowledge on the subject. The United Nations Conference on Climate Change, COP 21, took place in 2015 in Paris, where an agreement was adopted to strengthen the global response to the threat of climate change and to strengthen the capacity of countries to deal with the impacts arising from these changes. In 2022, at COP 27 in Egypt, the representatives of several countries gathered, aiming to reaffirm and expand the goals for reducing global warming.

These conferences highlight extreme weather events that populations may be increasingly exposed to, such as severe droughts, storms with intense flooding, cyclones, tornadoes and tsunamis in places where such phenomena were not common.

The emission of greenhouse gases from human activities, such as burning, deforestation and pollution, covers the Earth and retains the Sun's heat, leading to global warming and climate change. The world is currently warming faster than at any other time in recorded history [1].

The month of July 2023 was confirmed as the hottest month in the recent history of the Planet, following data released by the Copernicus Climate Change Service of the European Union. The average temperature was 16.95˚C, one and a half degrees above the level recorded in pre-industrial times. It is unlikely that the July record will remain an isolated fact this year [2].

A large amount of recent research points to the possibility of severe impacts arising from an increased frequency of extreme weather events. Scientists are already observing that the increase in the average temperature of the planet has raised sea levels due to the melting of the polar ice caps, which can cause the disappearance of islands and densely populated coastal cities. There are predictions of serious consequences for human populations and natural ecosystems, such as the extinction of animals and plants [1].

The oceans absorb more than 90% of the extra energy accumulated by retaining heat, due to greenhouse gases, and in the last few decades, since 1991, the temperature of the oceans has been increasing much faster [3]. As an effect, there are changes in the extent of sea ice, in the salinity of the sea and this negatively impacts all marine biota [4]. Furthermore, analyzes of oceanic data indicate that this energy gain has been modifying the behavior of the circulation of marine currents, the intensity, height and frequency with which the waves manifest themselves [5] [6] [7].

It thus becomes important to characterize the fluid dynamics in a warming climate. The classic Saint-Venant equations are widely used to describe fluid dynamics applied to many physical problems such as dam failure [8] [9], flooding [10], tsunami [11], urban drainage [12], and river flow [13], among others.

Usually, the solutions of these equations require the use of numerical and computational methods. Furthermore, the hyperbolic characteristic of the partial differential equations demands extra care to avoid spurious errors that impair the quality of the numerical solutions [14].

This article aimed to verify the influence of global warming on the dynamics of incompressible fluids, through the insertion of thermal energy in the Saint-

Venant equations. More specifically, the objectives were to computationally implement, via own codes in Octave, a finite volume method of the Lax-Friedrichs type, coupled to an Adams-Moulton type scheme, to simulate the temporal evolution of ocean waves; to involve the dynamics of the fluid in a medium characterized by the Earth's Troposphere and consider the transfer of thermal energy from the medium to the fluid in two distinct moments: first, without effects of global warming and then with effects of global warming.

The paper is organized as follows. Section 2 was intended for a brief presentation of the Saint-Venant equations, highlighting the modifications made to add the equations involving thermal energy and the distribution of ambient temperature. In Section 3, we describe the methods used to discretize the equations. The implemented simulations are in Section 4. Finally, in Section 5 we have the conclusions.

2. Modeling Mathematical

The classical Saint-Venant equations describe the flow of water as an incompressible, non-viscous and non-heat conducting fluid subject to free-surface gravity flow [8] [9].

The law of conservation of mass equation takes the form,

$$\frac{\partial h}{\partial t}+\frac{\partial}{\partial x}(uh)=0, \tag{1}$$

where $h=(x,t)$ is the total depth of the fluid (water height) whose reference is the bottom topography, and $u=u(x,t)$ is the velocity of the fluid in x-direction.

The conservation of momentum is given by,

$$\frac{\partial}{\partial t}(hu)+\frac{\partial}{\partial x}\left(hu^2+p\right)=-gh\frac{\partial z}{\partial x}, \tag{2}$$

in which the pressure term p is defined by $p=\frac{1}{2}gh^2$ under gravitational forces, g is the constant acceleration due to gravity and $z=z(x)$ describes the bottom topography.

The Equations (1) and (2) are also called the Shallow Water Equations. In this system can also be possible to consider another balance equation to describe the balance of energy [15],

$$\frac{\partial E}{\partial t}+\frac{\partial}{\partial x}\left(u\left(E+p\right)\right)=-ghu\frac{\partial z}{\partial x}, \tag{3}$$

where $E=E(x,t)$ is energy of system.

In this work, to add the influence of the increase in the temperature of the environment on the fluid dynamics, we will consider a fluid that receives thermal energy and is capable of changing its movement [16].

In this sense, we assume the dynamics of the fluid described by the Saint-Venant equations immersed in a medium. In this research, the interest is to investigate the propagation of ocean waves reaching the Earth's surface, so we adopted

the physical characteristics of the Earth's Troposphere and, therefore, the waves have heights that are compatible with this region. Most of the atmospheric phenomena are concentrated in the Troposphere and, in the neighborhood of its base, the atmospheric dynamics are complex, however, if we consider that, while the dynamics of the ocean wave develop, the atmospheric conditions remain static, we can use as a reference the International Standard Atmosphere (ISA) based on the U.S. Standard Atmosphere [17], which is a static atmospheric mathematical model, for describing the dependence of temperature, density and pressure on altitude.

In the atmospheric static model, in the Troposphere, the temperature of the medium in relation to altitude is given by an affine function and as we move away from sea level, the temperature decreases with height, creating a temperature distribution along the altitude.

At all times, the oceanic fluid will be in contact with the medium. We consider that such a medium behaves as a thermal reservoir, that is, the medium will transfer thermal energy to the fluid in a way that its temperature distribution is not affected. The heat transfer from the medium to the fluid adds energy to the system of Saint-Venant equations, influencing the horizontal displacement of the fluid and increasing the total energy of the system.

For this, the right side of Equation (2), adds to the kinematic heat flux given by Fourier's Law [18],

$$Q = -\kappa h \frac{\partial T}{\partial y},$$

in which κ is the kinematic thermal conductivity of the fluid (water) and $T = T(y)$ is the ambient temperature or environmental temperature. Furthermore, on the right side of Equation (3) thermal energy gain was included, transferred from the environment to the fluid by the term $\mathcal{H} = -\alpha\beta(T - T_{amb})$, which α is the heat exchange coefficient and T_{amb} is the average temperature of the environment (Earth planet) at sea level, in case T_{amb} (Kelvin).

To represent the different temperatures according to the height of the fluid, we defined a linear temperature distribution $T(y) = T_{amb} - 50\beta y$ to be influenced by T_{amb}. A modification T_{amb} causes both the temperature distribution and $\mathcal{H}$ to be affected by a factor β.

In this way, we can rewrite Equations (1), (2) and (3) on a system of partial differential equations in the form of a law of balance as follows

$$\boldsymbol{U}_t + \boldsymbol{F}(\boldsymbol{U})_x = \boldsymbol{S}(\boldsymbol{U}), \tag{4}$$

with

$$\boldsymbol{U} = \begin{bmatrix} h \\ hu \\ E \end{bmatrix}, \boldsymbol{F}(\boldsymbol{U}) = \begin{bmatrix} hu \\ hu^2 + \frac{1}{2}gh^2 \\ u\left(E + \frac{1}{2}gh^2\right) \end{bmatrix} \text{ and } \boldsymbol{S}(\boldsymbol{U}) = \begin{bmatrix} 0 \\ -gh\frac{\partial z}{\partial x} - \kappa h\frac{\partial T}{\partial y} \\ -ghu\frac{\partial z}{\partial x} - \alpha\beta(T - T_{amb}) \end{bmatrix}. \tag{5}$$

Equation (4) is a balance law whose vector $\boldsymbol{U}$ has the conserved variables, $\boldsymbol{F}(\boldsymbol{U})$ is a flux vector and $\boldsymbol{S}(\boldsymbol{U})$ is the source term vector. Except for very specific situations, analytical solutions are not available for the Saint-Venant equations and, basically, one numerical treatment is necessary to solve the System (4). When $\boldsymbol{S}(\boldsymbol{U})=0$, we obtain a conservation law that is a non-linear hyperbolic system of partial differential equations (PDEs) can be able to admit non-smooth solutions, requiring a lot of attention in choosing the numerical method [14].

The System (4) becomes well-posed when is defined initial and boundary conditions. The initial condition will represent a column of water at rest whose movement is started by gravitational forces and its function will be described in Section (4). On the boundaries, we have Neumann conditions, but under the bottom topography is necessary to put a hydrostatic equilibrium condition [10] given by

$$\frac{\partial}{\partial x}\left(\frac{1}{2}gh^2\right)=-gh\frac{\partial z}{\partial x}. \tag{6}$$

3. Numerical Methods

From a computational point of view, the challenge to obtain numerical solutions for System (4) is in the basic conservation law,

$$\boldsymbol{U}_t+\boldsymbol{F}(\boldsymbol{U})_x=0. \tag{7}$$

The source term $\boldsymbol{S}(\boldsymbol{U})$ has a numerical treatment standard, that is, we can split a partial differential equation (PDE) with source term in coupled equation: a homogeneous PDE and an ordinary differential equation [8]. For instance, we consider one-dimensional balance law $\boldsymbol{U}_t+\boldsymbol{F}(\boldsymbol{U})_x=\boldsymbol{S}(\boldsymbol{U})$, Equation (4), and split it in

$$\begin{cases}\boldsymbol{U}_t+\boldsymbol{F}(\boldsymbol{U})_x=0\\ \boldsymbol{U}(x,t_n)=\boldsymbol{U}^n\end{cases}\Rightarrow\bar{\boldsymbol{U}}^{n+1} \tag{8}$$

and

$$\begin{cases}\dfrac{\mathrm{d}\boldsymbol{U}}{\mathrm{d}t}=\boldsymbol{S}(\boldsymbol{U})\\ \boldsymbol{U}(x,t_n)=\bar{\boldsymbol{U}}^n\end{cases}\Rightarrow\boldsymbol{U}^{n+1}, \tag{9}$$

in which, first, to execute the temporal evolution of the EDP with source term, for a time t_n até t_{n+1}, the numerical solution of the homogeneous EDP is obtained (8), represented by $\bar{u}^{n+1}$. Then the numerical solution is updated by solving the ODE within the same time interval and using the solution $\bar{u}^{n+1}$ as initial condition. Finally, we obtain the numerical solution of the EDP (4) not homogeneous in time t_{n+1}.

To solve Equation (8), we use a finite volume method with the numerical flow of the Lax-Friedrichs type and Equation (9) was solved by the two-stage Adam-Moulton method.

3.1. Lax-Friedrichs Scheme

A Conversation Law (7) can be discretized in a control volume $\left[t^n, t^{n+1}\right]\times\left(x_{i-1/2}, x_{i+1/2}\right)$ the following conservative form [8] [9] [14]

$$U_i^{n+1} = U_i^n - \frac{\Delta t}{\Delta x}\left[F_{i+1/2}^n - F_{i-1/2}^n\right], \tag{10}$$

in which $F_{i+1/2}^n = \mathcal{F}\left(U_{i-p}^n, U_{i-p+1}, \cdots, U_{i+q}^n\right)$ is a numerical flux defined by each method which considers a regular partition of the spatial domain

$$\Omega_x : x_1 < \cdots < x_i < \cdots < x_{N+1},$$

with N subintervals in which

$$\Delta x = \frac{x_{i+1} - x_i}{N},$$

for any value of i existent. The i-th *average cell* or the i-th *finite volume* is defined by, $\Omega_i = \left(x_{i-1/2}, x_{i+1/2}\right)$ where $x_{i+1/2} = \frac{x_{i+1} + x_i}{2}$; note that each average cell has the size of the spacing Δx, because $x_{i+1/2} - x_{i-1/2} = \Delta x$.

Representing the conservation law with respect to the analytical solution by $u_t + f(u)_x = s(u)$, the values

$$U_i^n \cong \frac{1}{\Delta x}\int_{x_{i-1/2}}^{i+1/2} u\left(x, t_n\right)\mathrm{d}x = \frac{1}{\Delta x}\int_{\Omega_i} u\left(x, t_n\right)\mathrm{d}x \tag{11}$$

and

$$F_{i+1/2}^n \cong \frac{1}{\Delta t}\int_{t_n}^{t_{n+1}} f\left(u\left(x_{i+1/2}, t\right)\right)\mathrm{d}t. \tag{12}$$

are respectively, the approximate average value of the quantity u on the finite volume Ω_i in time t_n and the average value of the flow through $x_{i+1/2}$ between times t_n and t_{n+1}. The Lax-Friedrichs Method in the context of finite volume methods consists of approximating the flow $f(u)$ as a piecewise constant function, see Figure 1, that is,

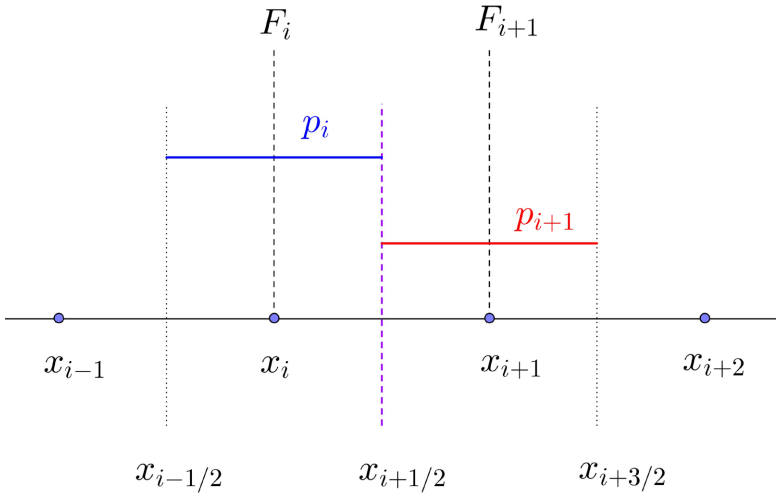

Figure 1. Graphical representation of the Lax-Friedrichs method where $f(u)$ is constant within each average cell Ω_i.

$$p_i(x) = U_i^n,\ x \in \left(x_{i-1/2}, x_{i+1/2}\right),$$

where $p_i(x) = U_i^0 = u(x,0)$ with $x \in \left(x_{i-1/2}, x_{i+1/2}\right)$, matches the initial condition.

In this way, it is possible to obtain approximations for the integrals defined in Equations (11) and (12), and obtain the classical form of the Lax-Friedrichs type finite volume method in conservative form (**Classical Lax-Friedrichs**),

$$U_i^{n+1} = \frac{1}{2}\left(U_{i-1}^n + U_{i+1}^n\right) - \frac{\Delta t}{2\Delta x}\left[F_{i+1/2} - F_{i-1/2}\right]$$

$$F_{i+1/2} = F\left(U_i^n, U_{i+1}^n\right) = \frac{\Delta x}{2\Delta t}\left(U_j^n - U_{j+1}^n\right) + \frac{1}{2}\left(f\left(U_j^n\right) + f\left(U_{j+1}^n\right)\right). \tag{13}$$

Details of the procedures for constructing the method can be found in [8] [9] [14].

3.2. Adams-Moulton Scheme

When considering the source term, we need to solve an ordinary differential equation for each point of the spatial mesh. For this, without loss of generality, we adopt an Initial Value Problem (IVP), known as *Cauchy* problem, defined by:

$$\begin{cases} \dfrac{\mathrm{d}x}{\mathrm{d}t} = f(t,x),\ t \in I \subset \mathbb{R} \\ x(0) = x_0 \end{cases}, \tag{14}$$

where $f : I \times \mathbb{R} \to \mathbb{R}$ is a known function and $x = x(t)$, $x : I \to \mathbb{R}$, the function to be found [19].

In the implicit two-point, second-order Adams-Moulton scheme, the approximate solution ξ_{i+1} is defined by

$$\xi_{i+1} = \xi_i + \frac{h}{2}\left[f\left(t_{i+1}, \xi_{i+1}\right) + f\left(t_i, \xi_i\right)\right], i = 0, \cdots, N-1. \tag{15}$$

This method is also known as the Implicit Trapezoidal Method. Note that in this method it is not possible to isolate ξ_{i+1} so that it is possible to obtain ξ_{i+1} recursively (iterative), causing a linear system associated with the Equation (15), which must be solved to find the values ξ_i, $i = 1, \cdots, N-1$. The range of absolute stability is given by $J = (-\infty, 0)$, [20].

An alternative to not having to solve the linear system is to use the prediction and correction technique. The technique consists of estimating ξ_{i+1} which is on the right side of Equation (15), through an explicit scheme and replacing it in the expression defining the implicit method. In this way, the predictor-corrector Adams-Moulton 2 Method whose prediction is performed by the Adams-Bashforth 2 method is as follows,

$$\begin{cases} \xi_{pred} = \xi_i + \dfrac{h}{2}\left[3f\left(t_i, \xi_i\right) - f\left(t_{i-1}, \xi_{i-1}\right)\right] \\ \xi_{i+1} = \xi_i + \dfrac{h}{2}\left[f\left(t_{i+1}, \xi_{pred}\right) + f\left(t_i, \xi_i\right)\right] \end{cases}, i = 1, \cdots, N-1. \tag{16}$$

This procedure will cause the range of absolute stability to change $J = (-2, 0)$.

Thus, splitting the Balance Law (4) in the Conservation Law (8) and the Ordinary Differential Equation (9), applying the classical Lax-Friedrichs Scheme (13) in (4) and the Adams-Moulton Method (16) in (9), we are able to make numerical simulations to analysis the impact of ambient temperature under the water displacement dynamics describes by Saint-Venant equations.

4. Simulations and Results

In this section, three scenarios are performed, according to the following situations: Scenario 1 considers the Classical Saint-Venant equations, Equations (1) and (2) with bottom topography equal to zero and the initial condition for water level equal to a Gaussian function; Scenario 2 adopts a topography equal a hyperbolic tangent function and a constant initial level for water and Scenario 3 take the complete system, that is, the Sain-Venant equation with energy balance including the thermal energy transferred from environmental to water. In this last scenario, the bottom topography is equal to Scenario 2 and the water level is equal to Scenario 1.

All simulations have spatial domain computational given by $[-50,300]$, with $\Delta x = 350/1024$. For time discretization was taken $\Delta t = 0.01\Delta x$ in order to keep the numerical methods stable.

4.1. Scenario 1

Initially, the water level is described by

$$h(x,0) = 0.2 + \mathrm{e}^{-x^2/8} \tag{17}$$

whose initial velocity is zero. Also, in this case, the topography is $z(x) = 0$. In Figure 2, we plotted the initial water level by magenta color and performed its temporal evolution to $N_t = 100$, 500, 1000, 2000 and 5000 interactions, represented by blue color.

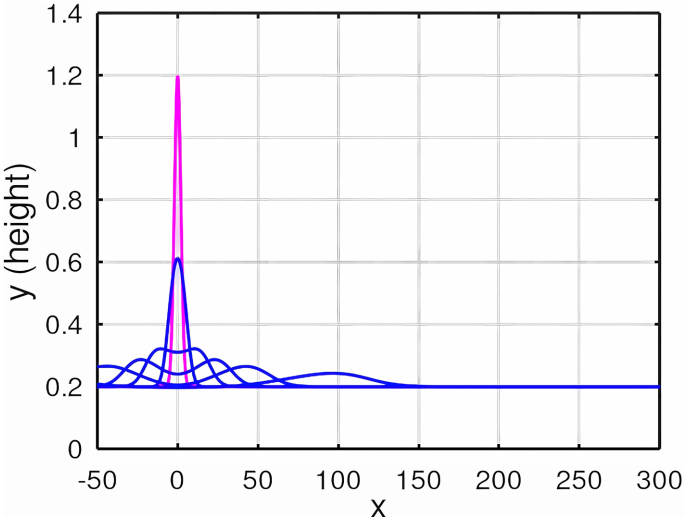

Figure 2. Initial condition (magenta color) and numerical solutions for classical Saint-Venant equations (blue color).

In Figure 2, the initial column water (magenta color) starts to be influenced by gravitational forces and its maximum point is diminished, making to waves that displace to opposite sides. Such behavior is expected and is in accordance with the literature, showing that the developed code itself is robust.

4.2. Scenario 2

In this scenario we have a bottom topography and an initial flat water level and such a description can be to represent a flood problem when we initially have immersed all bottom topography. The initial water suffer influences of the gravitational forces and the geometry of bottom topography, making the system dynamic.

For this example, it is necessary to include the hydrostatic equilibrium on topography, Equation (6), otherwise, the gravitational forces will able to dig the water in topography and, it is not desirable at this moment. Such topography is taken

$$z(x) = 0.1 + 0.1\tanh(x - 50), \tag{18}$$

and it is plotted in black color on the Figures 3-6. For this instance, the initial water level is $h(x,0) = 0.2$.

Figure 3 shows the interactions between $N_t = 100$, 500 and 1000. Notice that, the gravitational forces attract the water to the bottom topography, creating a valley at $x = 50$ and moving the fluid in opposite directions. The hydrostatic equilibrium condition prevents water from penetrating into the ground. When we continue the simulation, it is noticed that, when pulling the fluid downwards, a ridge is formed to the right, which continues its movement until it leaves the spatial domain, leaving a small elevation of water at the bottom of the topography. This is

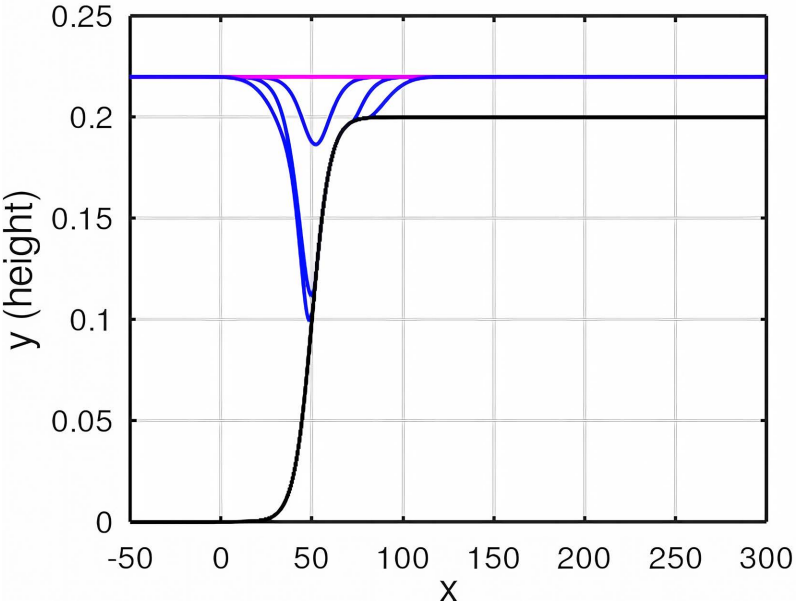

Figure 3. Initial condition (magenta color) and numerical solutions for classical Saint-Venant equations (blue color).

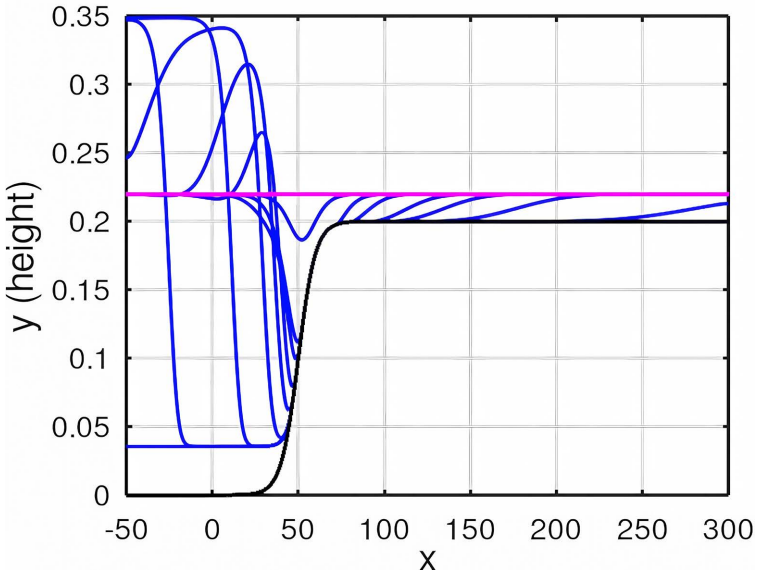

Figure 4. Initial condition (magenta color) and numerical solutions for classical Saint-Venant equations (blue color).

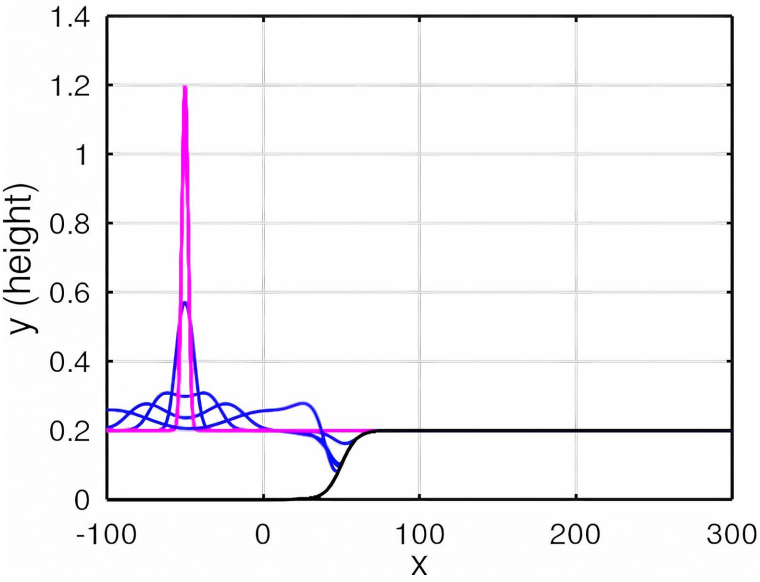

Figure 5. Initial condition (magenta color) and numerical solutions for complete Saint-Venant equations without global warming (blue color).

seen in **Figure 4**, which contains the interactions $N_t = 100$, 500, 1000, 2000, 3000, 5000, 10,000, 20,000 and 30,000.

4.3. Scenario 3

This scenario considers the Saint-Venant equations complete, that is, with terms involving thermal energy, System (4) with bottom topography and its hydrostatic equilibrium condition, Equation (6). For initial water level and for topography, we adopt the non-zero functions of Scenarios 1 and 2, respectively.

The realization of the temporal evolution of ocean waves in this scenario de-

pends on the characterization of the medium where the fluid dynamics are inserted. In Section (2) we describe such a medium adopting the profile of the Earth's Troposphere, whose temperature distribution in this medium is represented by the function $T(y) = T_{amb} - 50\beta y$.

The history of an average ambient temperature of 297 K ($T_{amb} = 24^{\circ}\mathrm{C}$) is compatible with some regions of planet Earth located between the tropics of Cancer and Capricorn, and this region of the planet is the one that is more susceptible to the consequences of climate change [1] [7].

If such a temperature is associated with an average that has not yet changed due to global warming, then the factor β does not have the effect of amplifying the temperature gradient and, therefore, we have $\beta = 1$. The values $k = 0.61$ and $\alpha = 1$ are characteristic of the water fluid [16] [18].

Based on the assumptions described, a first simulation was performed. **Figure 5**, $N_t = 100$, 500, 1000 and 2000, shows an initial Gaussian wave (magenta color) influenced by the gravitational force, decreasing its peak and subdividing it into two oceanic waves, moving in opposite directions. As the dynamic develops, the contact between the water and the soil suffers a retreat, forming a valley in $x \cong 50$. The part of the initial wave that started to move to the right, reaches the region of the valley and tries to overcome it.

The continuity of the dynamics is in **Figure 6**, $N_t = 2000$, 3000, 4000 and 10,000, where it is verified that the sea wave begins to expand through the valley (decreasing its depth), arrives close to the terrestrial level of $y = 0.2$, but cannot advance and it ends up being reflected to the left, not reaching the continent (represented by the topography of $y = 0.2$).

In this simulation, the potential energy of the falling initial wave is converted into the kinetic energy ocean wave at right, in addition to the thermal energy

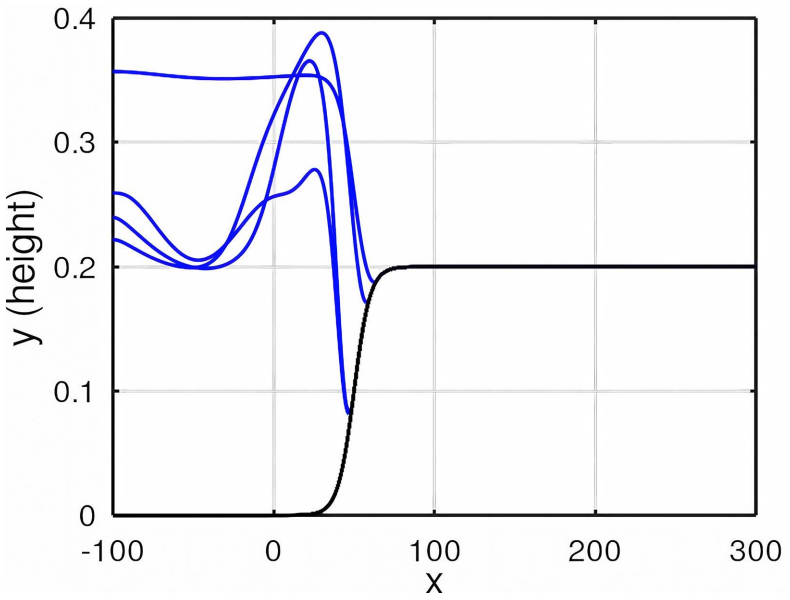

Figure 6. Numerical solutions for complete Saint-Venant equations without global warming (blue color).

transferred from the medium to the fluid displacement, did not generate wave dynamic capable of invading the continent.

For a second simulation, when considering the effects of global warming, the ambient temperature is changed and consequently the temperature gradient of the system. In the reference [21], it is estimated that for every degree change in the average temperature of the environment, the temperature gradient is doubled. Thus, if we consider that global warming has raised the average temperature of the environment we are considering by two degrees, we will have $T_{amb} = 299\,\mathrm{K}$ and $\beta = 4$ (two units for each degree raised).

Initially, we have the same wave (magenta color) from the previous simulation, **Figure 7** for $N_t = 100$, 500 and 1000. However, when developing the fluid dynamics in this new configuration of the medium, decreasing the peak and subdividing it into two waves, a displacement to the right is noticed due to the extra gain of thermal energy, converted into kinetic energy.

This way, the wave has enough energy to reach and overcome the valley, reaching and advancing over the continent in $y = 0.2$, see **Figure 8**, $N_t = 1000$, 2000, 3000, 4000 and 10,000.

The results obtained evidence that the advance of water on the continent is due to the increase in the average temperature of the environment, arising from global warming.

This reveals what can happen if established authorities do not take action to slow down climate change and global warming. Such effects can be verified in more detail in **Figure 9**, which is a zoom of **Figure 8**.

Catastrophic implications can emerge with the advance of ocean waters over the continent. Coastal cities tend to disappear, forcing the displacement of populations; natural nurseries of different species will be eliminated; flooding and destruction of food cultivation areas, among others.

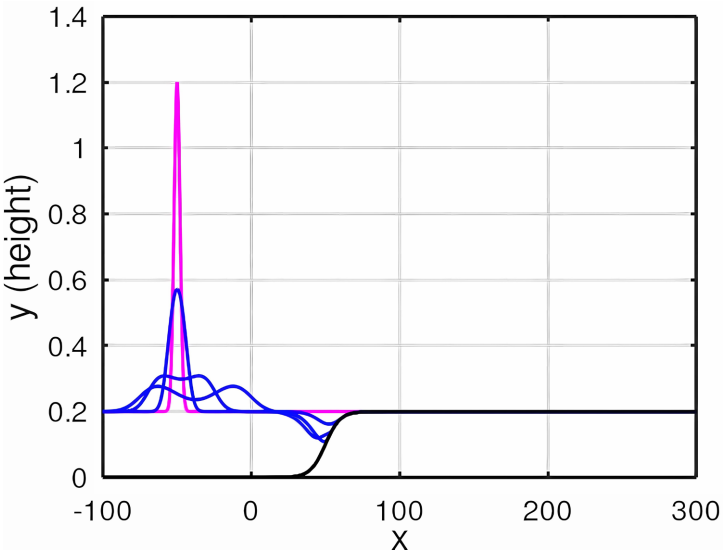

Figure 7. Initial condition in magenta color and numerical solutions in blue color for complete Saint-Venant equations with global warming.

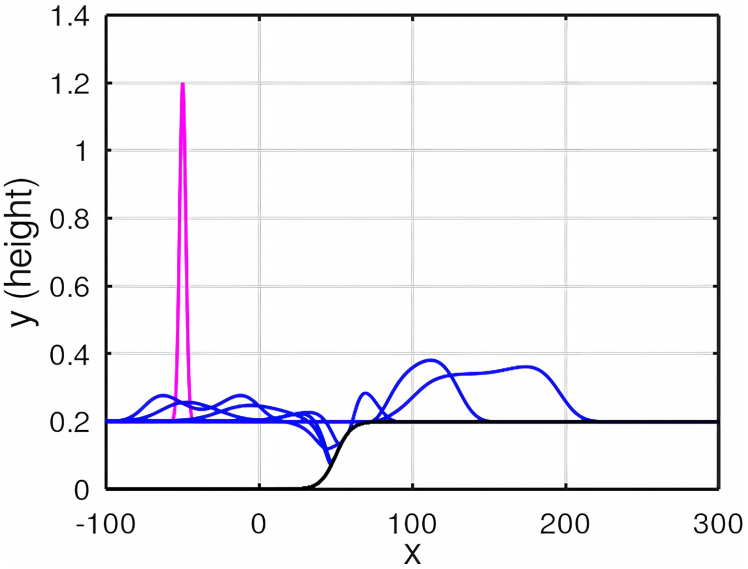

Figure 8. Initial condition (magenta color) and numerical solutions for complete Saint-Venant equations with global warming (blue color).

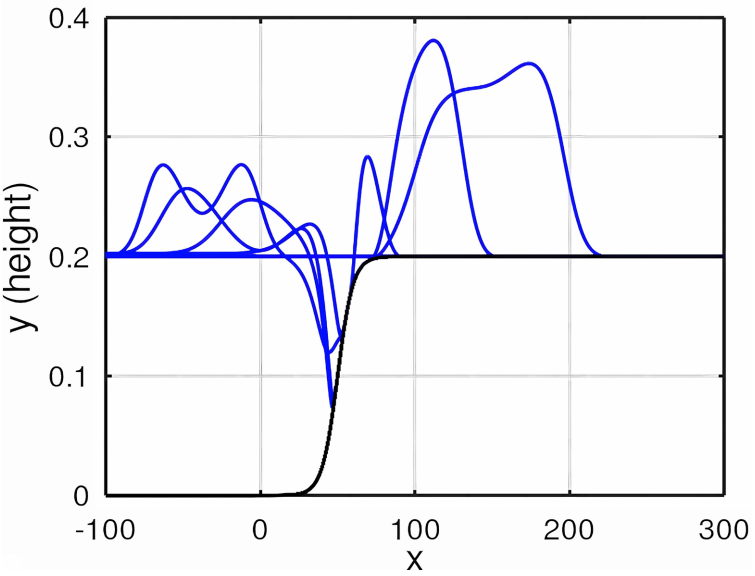

Figure 9. Numerical solutions for complete Saint-Venant equations with global warming (blue color).

5. Conclusions

Currently, the populations in different countries and continents are experiencing changes in temperature and climate patterns. These changes may be natural, however, since the 18th century human activities have been the main cause of climate change, mainly due to the burning of fossil fuels (such as coal, oil and gas), which produce gases that retain heat. As a consequence, increases in average ambient temperatures are taking place.

The purpose of this research was to add thermal energy to the Saint-Venant equations, which model the displacement of a fluid under the action of gravita-

tional force, in order to analyze the impact caused by global warming on the dynamics of the system.

Scenario simulations were implemented via the Lax-Friedrichs method coupled with the two-stage Adams-Moulton method. The results obtained in scenarios 1 and 2 showed that the numerical methods are robust, which made it possible to determine stable numerical solutions. Scenario 3 considers a complete system, with a description of the thermal energy capable of modeling the increase in temperature distribution in the environment. The transfer of thermal energy from the environment to the fluid can cause to advance of water towards the continent, in regions where this did not previously occur.

In this sense, it is important that measures are taken by the authorities of the countries, in order to brake the increase in temperatures on the planet.

Conflicts of Interest

The authors declare no conflicts of interest regarding the publication of this paper.

References

[1] Zandalinas, S.I., Fritschi, F.B. and Mittler, R. (2021) Global Warming, Climate Change, and Environmental Pollution: Recipe for a Multifactorial Stress Combination Disaster. *Trends in Plant Science*, **26**, 588-599. https://doi.org/10.1016/j.tplants.2021.02.011

[2] Pivetta, M. (2023) Julho de 2023 foi o mês mais quente na história recente do Planeta. Revista Pesquisa FAPESP.

[3] Albouy, C., *et al.* (2020) Global Vulnerability of Marine Mammals to Global Warming. *Scientific Reports*, **10**, Article No. 548. https://doi.org/10.1038/s41598-019-57280-3

[4] Laufkötter, C., Zscheischler, J. and Frölicher, T.L. (2020) High-Impact Marine Heatwaves Attributable to Human-Induced Global Warming. *Science*, **369**, 1621-1625. https://doi.org/10.1126/science.aba0690

[5] Reguero, B.G., Losada, I.J. and Méndez, F.J. (2019) A Recent Increase in Global Wave Power as a Consequence of Oceanic Warming. *Nature Communications*, **10**, Article No. 205. https://doi.org/10.1038/s41467-018-08066-0

[6] Widlansky, M.J., Long, X.Y. and Schloesser, F. (2020) Increase in Sea Level Variability with Ocean Warming Associated with the Nonlinear Thermal Expansion of Seawater. *Communications Earth & Environment*, **1**, Article No. 9. https://doi.org/10.1038/s43247-020-0008-8

[7] Bromirski, P.D. (2023) Climate-Induced Decadal Ocean Wave Height Variability from Microseisms: 1931-2021. *Journal of Geophysical Research*: *Oceans*, **128**, e2023JC019722. https://doi.org/10.1029/2023JC019722

[8] Toro, E.F. (1999) Riemann Solvers and Numerical Methods for Fluid Dynamics: A Practical Introduction. Springer Verlag, Berlin. https://doi.org/10.1007/978-3-662-03915-1

[9] Leveque, R.J. (2002) Finite Volume Methods for Hyperbolic Problems. Cambridge University Press, Cambridge. https://doi.org/10.1017/CBO9780511791253

[10] Kader, M.Y.A., Badé, R. and Saley, B. (2020) Study of the 1D Saint-Venant Equa-

tions and Application to the Simulation of a Flood Problem. *Journal of Applied Mathematics and Physics*, **8**, 1193-1206. https://doi.org/10.4236/jamp.2020.87090

[11] Curcic, M. (2020) Modern Fortran, Building Efficient Parallel Applications. Manning, Shelter Island.

[12] Hodges, B.M. (2019) Conservative Finite-Volume Forms of the Saint-Venant Equations for Hydrology and Urban Drainage. *Hydrology Earth System Sciences*, **23**, 1281-1304. https://doi.org/10.5194/hess-23-1281-2019

[13] Feng, D., Tan, Z. and He, Q. (2023) Physics-Informed Neural Networks of the Saint-Venant Equations for Downscaling a Large-Scale River Model. *Water Resources Research*, **59**, e2022WR033168. https://doi.org/10.1029/2022WR033168

[14] Kurganov, A. (2018) Finite-Volume Schemes for Shallow-Water Equations. *Acta Numerica*, **27**, 289-351. https://doi.org/10.1017/S0962492918000028

[15] De Vuyst, F. (2021) Efficient Solvers for Shallow-Water Saint-Venant Equations and Debris Transportation-Deposition Models. Cornell University, Ithaca.

[16] Giovangigli, V. and Tran, B. (2010) Mathematical Analysis of a Saint-Venant Model with Variable Temperature. *Mathematical Models and Methods in Applied Sciences*, **20**, 1251-1297. https://doi.org/10.1142/S0218202510004593

[17] National Aeronautics and Space Administration (1976) U.S. Standard Atmosphere. U.S. Government, Washington DC, NASA-TM-X-74335.

[18] Nussenzveig, H.M. (2009) Curso de física básica. Volume 2, Blutcher, São Paulo.

[19] Garcia, R.O. and Silveira, G.P. (2018) Numerical Solutions of ODEs Applied in the Study of Population Dynamics. *C.Q.D. Revista Eletrônica Paulista de Matemática*, **13**, 46-69. https://doi.org/10.21167/cqdvol13201823169664roggps4669

[20] Buchanan, J.L. (1992) Numerical Methods and Analysis. McGraw Hill, Singapore.

[21] Furtado, M.T. (2012) Adiabatic Model of the Earth's Atmosphere Compatible with the Greenhouse Effect. *Revista Brasileira de Ensino de Física*, **34**, 1-13. https://doi.org/10.1590/S1806-11172012000300010